Estimation of the temperature field on a composite fan cowl using the static capacity of surface-mounted piezoceramic transducers

Emmanuel Lize, Marc Rebillat, Nazih Mechbal, Christian Bolzmacher

Estimation of the temperature field on a composite fan cowl using the static capacity of surface-mounted piezoceramic transducers.

Emmanuel LIZÉ*. Marc RÉBILLAT.**
Nazih MECHBAL. Christian BOLZMACHER***

*CEA, LIST, Sensorial and Ambient Interfaces Laboratory,
91191 - Gif-sur-Yvette CEDEX, France.
**Processes and Engineering in Mechanics and Materials Laboratory
(PIMM, UMR CNRS 8006, Arts et Métiers ParisTech (ENSAM)),
151, Boulevard de l'Hôpital, Paris, F-75013, France.
(e-mail: emmanuel.lize@cea.fr)

Abstract: The influence of temperature on SHM (Structural Health Monitoring) systems using guided waves is a major problem for their industrial deployment. One of the cheapest SHM process developed in aeronautical context is based on piezoelectric transducers mounted on the monitored structure. Several methods are used to assess the presence of damage. A popular one is based on tracking changes in the electromechanical impedance of the transducers: it is an efficient damage indicator around the device and can also be used as a fault diagnosis indicator for the transducer itself. However, monitoring decisions need to be robustified with temperature sensors also mounted on the structure. In this article, the electromechanical impedance is used to determine the temperature on each lead zirconate titanate transducer (PZT). This avoids supplementary instrumentation and the entire temperature field of the structure is estimated. The proposed approach is tested experimentally on a on a small composite plate and then on a real part of an A380 composite nacelle. Results show that the temperature field on the structure can be estimated with a precision of ± 5 °C using a linear regression between static capacity and temperature.

Keywords: aerospace, health monitoring and diagnosis, smart sensors and actuators, networks of sensors and actuators, piezoceramic devices, temperature effect, electromechanical signature.

1. INTRODUCTION

SHM is an important field for aeronautical industries. The revolution of new technologies and the increasing interest for composite materials and piezoceramic devices lead to the creation of light and large smart structures able to give relevant auto-diagnosis for SHM processes.

Guided wave is a popular method for damage detection and localization. Lead zirconate titanate transducer (PZT) mounted on the structure being monitored is a cheap and easy-to-settle method to trigger and detect waves using the PZT as sensor and actuator. A damage can be detected by comparing measurements of a damaged structure against measurements of the same structure in a pristine state. The resulting signal strongly depends on the structure's mechanical properties which are significantly altered in presence of damage or when temperature varies. Therefore, a temperature variation as small as 2 °C can lead to false damage detection (Marzani and Salamone, 2012; Putkis et al., 2015). However, a good knowledge of the influence of temperature on the signal used allows one to compensate efficiently for its variations (Fendzi, 2015; Wang and al., 2014; Konstantinidis and al., 2006; Lu and Michaels, 2005). For these techniques to work, a lot of temperature sensors are then needed to measure temperature on each possible path between the PZTs of the structure. In an aeronautical context where large structures are exposed to varying and heterogeneous temperatures fields, it means adding extra sensors and wires. The main idea proposed here is that the additional weight of these sensors and wires can be avoided by using temperature estimation provided directly by PZT transducers which are already mounted on the structure.

The electromechanical (EM) signature of PZT devices is the impedance of PZTs coupled to the structure under test. This measurement has gained importance in the SHM community (Park et al., 2006, 2003; Annamdas and Soh, 2010) because it can be used as a damage detection method and to evaluate the health degradation of a PZT or its boundary conditions. The influence of temperature on the EM signature of PZTs has been the focus of several research teams. Experimental (Lin et al., 2010; Qing et al., 2008; Yang et al., 2008) and numerical studies (Sepehry et al., 2011; Yang and Miao, 2008) pointed out that the static capacity of a PZT increases, and the modal frequencies are lowered for increasing temperatures (Balmes et al., 2014; Grisso and Inman, 2010; Overly et al., 2009). Temperature compensation methods have been proposed based on those observations, and studies have been carried out to distinguish effects attributable to the presence of damage from those due to temperature variations (Grisso and Inman,

2010; Overly et al., 2009; Koo et al., 2008; Zhou et al., 2009). All these studies are efficient in proving the sensitivity of PZT to temperature, but very few works have been carried out to use the PZT as temperature sensors as we would like to do here. For instance (Ilg et al., 2013) describes the use of the static capacity of air coupled ultrasound transducers to estimate the temperature of a structure with a precision of ±4.5 °C. Our previous work (Lize et al., 2016) showed good temperature estimation results (±2 °C) on a composite plate but was only realized under homogeneous temperature fields.

The temperature estimation procedure developed in this article is based on a linear regression of the static capacity of the PZT mounted on a structure for varying temperature. This approach will first be applied on a composite plate under heterogeneous temperature field, and then on a large A380 fan cowl (real part of an airplane nacelle) made of the same composite material.

2. STATIC CAPACITY

2.1 Theoretical background

A PZT mounted on a structure can be qualified by its electro-mechanical signature. The impedance Z of a PZT is defined as the transfer function between the voltage V applied to the PZT element and the resulting electrical current I. The static capacity C is defined as the imaginary part of the admittance $Y(\omega)$ (inverse of the impedance) divided by ω, ω denoting the angular frequency.

$$C = \frac{\mathrm{Im}(Y(\omega))}{\omega} \qquad (1)$$

$$\text{with } Y(\omega) = \frac{1}{Z(\omega)} = \frac{I(\omega)}{V(\omega)}$$

A piezoelectric material is characterized by its electric field strength E and the electric charge density displacement D. The linear electrical behavior of the material and the Hooke's law lead to the following coupled equations:

$$\begin{cases} \varepsilon = s^E \sigma + d^T E \\ D = d\sigma + \epsilon^\sigma E \end{cases} \qquad (2)$$

where ε is the strain, σ is the stress, d is the matrix of direct piezoelectric effect, d^T is the matrix of the converse piezoelectric effect, s^E is the matrix of the elastic compliance at constant electric field, and ϵ^σ is the matrix of permittivity at constant stress field.

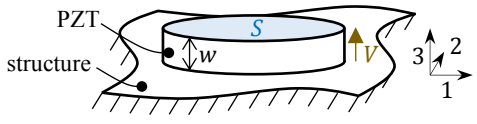

Fig. 1. Circular PZT bounded to a rigid structure

In our case-study, thin circular PZTs are mounted on a rigid structure (Fig. 1) experiencing no deformation in the plane direction ($\varepsilon_1 = \varepsilon_2 = 0$), and are un-constrained in the out-of-plane direction ($\sigma_3 = 0$). The electric charge density displacement can then be written as:

$$D_3 = d_{31}(\sigma_1 + \sigma_2) + \epsilon_3^\sigma E_3 \qquad (3)$$

$$\text{with } \sigma_1 = \sigma_2 = -\frac{\tilde{E}}{1-\upsilon_{12}} d_{31} E_3$$

$$\text{and } E_3 = \frac{V}{w}$$

where V is the voltage applied to the PZT, w is the thickness of the PZT, $\tilde{E}$ and υ_{12} are respectively the Young's modulus and Poisson's coefficient of the PZT in direction 1 and 2. The capacity of the PZT bounded to the structure C_b is then defined by:

$$C_b = \frac{SD_3}{V} = \frac{S}{w}\left(\epsilon_3^\sigma - 2\frac{\tilde{E}\cdot d_{31}^2}{1-\upsilon_{12}}\right) \qquad (4)$$

where S is the surface of the PZT.

A free PZT (not bounded to the structure) is not constrained ($\sigma_1 = \sigma_2 = 0$) which means that its capacity C_f is only defined by:

$$C_f = \frac{S\epsilon_3^\sigma}{w} \qquad (5)$$

The capacity of the bounded PZT can then be expressed as:

$$C_b = C_f - K_b \qquad (6)$$

$$\text{with } K_b = \frac{2S}{w}\left(\frac{\tilde{E}\cdot d_{31}^2}{1-\upsilon_{12}}\right)$$

This value of the capacity is purely theoretical, obtained considering a totally rigid structure and a perfect bonding. In practice, the value of the capacity should be included between C_b and C_f for a healthy PZT. The variation of the relative permittivity with temperature is given by the constructors. For soft piezoceramic of type 5A, this variation can be considered as linear on a limited range of temperature. The permittivity in terms of temperature θ can be expressed as:

$$\epsilon_3^\sigma(\theta) = \epsilon_3^{\sigma,\theta_{ref}} \times \left[1 + \alpha_\epsilon\left(\theta - \theta_{ref}\right)\right] \qquad (7)$$

where θ_{ref} states for the temperature of reference at which the PZT parameters are defined and α_ϵ the temperature coefficient for permittivity.

Bounding a PZT to a structure causes a drop of its capacity (compared to free conditions). When the bounding is perfect, the slope of the capacity variation with temperature is the same for a free or bounded PZT. It means that the term K_b in (6) does not depend on temperature.

The capacity of the PZT in terms of temperature is calculated using (4) and (7):

$$C(\theta) = C^{\theta_{ref}} + \alpha_c \left(\theta - \theta_{ref}\right) \quad (8)$$

$$\text{with } \alpha_c = \frac{S}{w}\alpha_c$$

where α_C is the temperature coefficient for capacity and $C^{\theta ref}$ is the static capacity at θ_{ref}. We use (8) to compute an estimation of the temperature $\hat{\theta}_{estim}$ from any static capacity measurement C_{meas}:

$$\theta_{estim} = \frac{C_{meas} - C_b^{\theta_{ref}}}{\alpha_c} + \theta_{ref} \quad (9)$$

2.2. Experimental approach

In the experimental approach, the static capacity is the mean of the capacity obtained from voltage and intensity measurements on a range of frequencies (ω_a to ω_b):

$$C = \frac{1}{\omega_b - \omega_a}\int_{\omega_a}^{\omega_b} \frac{\mathrm{Im}\left(\frac{V(\omega)}{I(\omega)}\right)}{\omega} d\omega \quad (10)$$

Coefficients α_C and $C^{\theta ref}$ are determined by applying a linear regression on reference capacity measurements realized at different temperatures (Lize et al., 2016). The linear regression quality is evaluated with the coefficient of determination r^2. This indicator is contained between 0 (erroneous regression) and 1 (perfect fit). The estimation temperature error is given by the difference between the estimated temperature $\hat{\theta}_{estim}$ and the measured temperature θ_{meas}.

3. EXPERIMENTS ON A COMPOSITE PLATE

Before applying the approach on real airplane parts, experiments have been performed on a small plate of the same anisotropic composite material.

A CFRP plate of four plies $[0°/-45°/45°/0°]$ of 0.28 mm each was used for the first experiments. It was instrumented with five Noliac NCE51 PZT (diameter: 20 mm, thickness: 0.5 mm, Curie temperature: 360 °C) and glued with a Redux 322 epoxy adhesive (operating temperature range from −55 °C to 200 °C). Impedance measurements were realized with a Hioki IM3570 impedance analyser and data processed with Matlab. The static capacity was then computed using (10) with 800 impedance measurements between 20 kHz and 60 kHz acquired 3 times to increase the signal to noise ratio (SNR).

Previous studies on a composite plate with the same dimensions and properties have shown that a linear regression can be applied to the variation of static capacity with temperature. In this previous case, measurements had been done between 10 and 60 °C to determine the linear regression coefficients (Lize et al., 2016).

Before one uses the PZT as temperature sensors, the linear regression parameters α_C and C^0 are determined under controlled temperature variations to create the database. In this study, they are determined for each PZT on the structure with experimental measurements of static capacity realized at only three different temperatures: 22, 35 and 42 °C (see Table 1).

Table 1. Linear regression parameters and coefficient of determination of the capacity variation with temperature for the five PZT of the composite plate.

	PZT1	PZT2	PZT3	PZT4	PZT5
$\alpha_C \times 10^{-11}$(F/°C)	1.32	1.30	1.40	1.34	1.37
$C^0 \times 10^{-9}$(F)	7.38	7.38	7.22	7.22	7.39
r^2	0.98	0.99	0.99	1	1

It can be noticed from Table 1 that the coefficients α_C for each PZT are close to each other, but a small difference is observable because they do not have exactly the same boundary and ageing conditions. The theoretical value of the capacity C^0 is obtained with parameters supplied by NOLIAC and using (5) and (6): it equals 9.58 nF for a free PZT and 4.00 nF for a perfectly bounded one. The experimental capacities from Table 1 are contained between these two values which makes sense because when the bonding conditions get worth, the transducers tend to behave like a free PZT. The coefficients of determination r^2 are high, meaning that the linear regression is well fitted, but this result should be interpreted with great care considering that only three measurements were used to get the coefficients. With this database containing the regression coefficient for each PZT (Table 1), it is possible to estimate the temperature of the monitored plate under heterogeneous temperature fields (spatial temperature gradient). The temperature field is applied with an infrared lamp of 300 W placed one meter away from the structure and captured using a thermal camera.

Fig. 2 and Table 2 shows an example of results obtained for a temperature field applied on the composite plate.

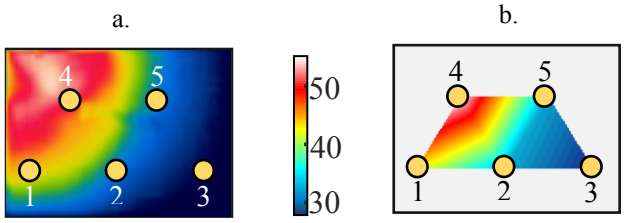

Fig. 2. Temperature field (in °C) on the composite plate obtained with the thermal camera (a.) and estimated using the static capacity measurements (b.)

Table 2. Temperature measured with the thermal camera (θ_{meas}) and estimated with the static capacity ($\hat{\theta}_{estim}$) on PZT locations corresponding to Fig. 2

PZT	1	2	3	4	5
θ_{meas} (°C)	40,5	32,4	27,6	50,4	32,4
$\hat{\theta}_{estim}$ (°C)	43,4	32,8	28	55,4	32,2

4. EXPERIMENT ON THE FAN COWL

4.1 The structure

The fan cowl is part of the structure embracing the plane reactor. In practice, it is exposed to heterogeneous temperature variation from −40 to 150 °C (Fendzi, 2015). The large dimensions of this CRFP structure against thickness (diameter: 3.90 m, height: 2.10 m, thickness: 1.12 mm) suggests that the behaviour of lamb waves in the fan cowl will be very close to the one in the plate. It is monitored with 30 Noliac NCE51 PZT patches (diameter: 25 mm, thickness: 0.5 mm) glued with a Redux 322 epoxy adhesive (Fig. 3a). For experiments, only nine PZT in the blue test zone have been used with positioning as indicated in Fig. 3b.

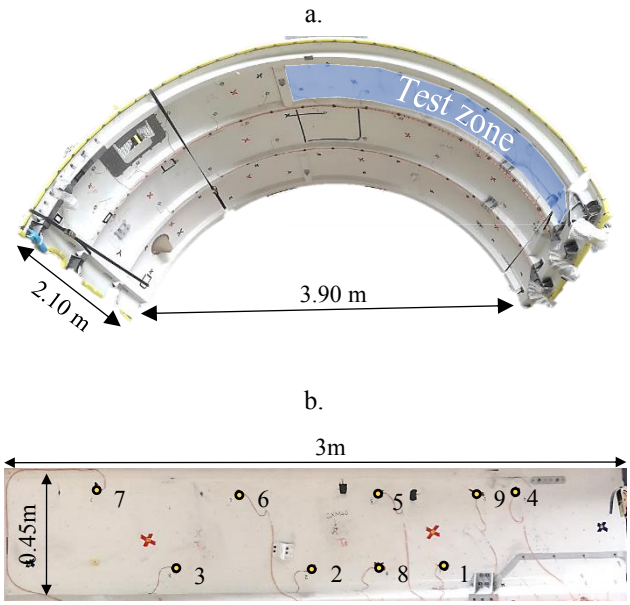

Fig. 3. Fan cowl monitored by 30 PZTs (a.) and focus on the test zone used for experiments in this article (b.)

4.2 Creation of the database

Table 3. Regression coefficients and coefficient of determination for the 8 healthy PZT of the test zone

	PZT1	PZT2	PZT3	PZT4
$\alpha_C \times 10^{-11}$ (F/°C)	1.84	1.77	1.16	2.35
$C^0 \times 10^{-9}$(F)	11.3	11.6	11.7	11.5
r^2	1	1	1	1

	PZT6	PZT7	PZT8	PZT9
$\alpha_C \times 10^{-11}$ (F/°C)	1.55	1.16	1.66	2.74
$C^0 \times 10^{-9}$(F)	11.5	10.6	10.4	10.3
r^2	0.96	1	1	1

The temperature of the fan cowl could not be easily monitored because of the unavailability of an environmental chamber large enough for such structure. Therefore, the database was created using 245 measurements realised at ambient temperatures from 15 to 21 °C during three consecutive days to determine the regression coefficient for each PZT (see Table 3). The PZT 5 is not included in the results because a first auto-diagnostic based on the impedance has shown that it is damaged (faulty sensor).

4.3 Experiments with homogeneous temperature

First experiments have been performed under a homogeneous temperature field on the complete test zone to check the applicability of this technique on a large structure. 54 measurements that were not used for the database creation with temperatures between 15 and 21 °C were used. Fig. 4 shows the error distribution of the temperature estimation computed for each PZT. For this temperature range, an equivalent precision as on the plate under homogeneous temperature was found (±2 °C).

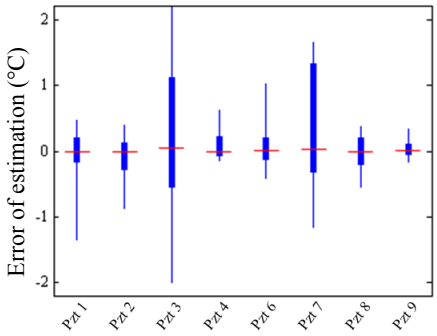

Fig. 4. Error of temperature estimation for the 8 healthy PZTs obtained on 54 random measurements between 15 and 21 °C.

4.4 Experiments with heterogeneous temperature fields

Previous experiments and the temperature field estimated on the composite plate let suppose that a heterogeneous temperature field can be estimated on the fan cowl.

Different temperature field configurations have been tested on the test zone by placing the infrared light at various positions. Real temperatures at the PZT transducer locations are determined with the FLIR software which allowed us to measure the real temperature of the structure under test on precise points of the image. Three thermal images are taken on the test zone for a better precision. The structure was heated 20 minutes with the infrared lamp before the measurements were realised to make sure that the temperature field is stable.

The following results of two tests (Fig. 5 and Fig. 6) show the temperature field obtained with the thermal camera and the temperature field obtained with the static capacity of the PZT using the same colour scale for temperature. Images obtained with the static capacity agree with the ones of the thermal camera. However, the temperature field obtained with the PZT is slightly less precise because it is obtained with less estimation points.

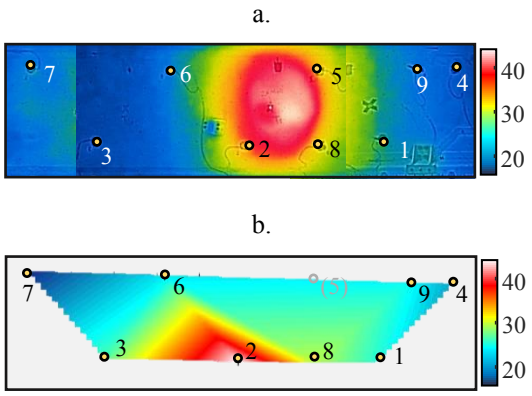

Fig. 5. First configuration of the temperature field. Temperature field obtained with the thermal camera (a.) and with the static capacity of PZT (b.)

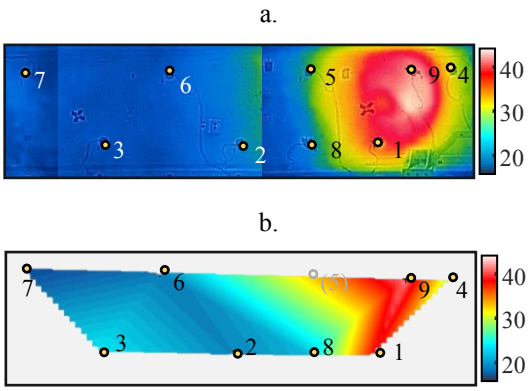

Fig. 6. Second configuration of the temperature field. Temperature field obtained with the thermal camera (a.) and with the static capacity of PZT (b.)

Table 4. Temperature measured with the thermal camera (θ_{meas}) and estimated with the static capacity ($\hat{\theta}_{estim}$) on PZT locations corresponding to Fig. 5

PZT	1	2	3	4	6	7	8	9
θ_{meas} (°C)	24	37	22	20.3	22.3	17.6	26.6	24
$\hat{\theta}_{estim}$ (°C)	24.2	41.2	25.2	20.2	22.9	16.7	28.2	23.5

Table 5. Temperature measured with the thermal camera (θ_{meas}) and estimated with the static capacity ($\hat{\theta}_{estim}$) on PZT locations corresponding to Fig. 6

PZT	1	2	3	4	6	7	8	9
θ_{meas} (°C)	32	17.2	20	28.7	18.5	17.8	20.7	42
$\hat{\theta}_{estim}$ (°C)	38.5	18.7	22.4	28.1	18.2	16.1	20.6	41.7

5. DISCUSSION

The hysteretic behaviour observed by (Ilg et al., 2013) has been noticed on measurements realised on the fan cowl. During the three days of measurements, the static capacity varied linearly with temperature but with different slopes depending on the temperature variation direction. In previous works (Lize et al., 2016), a precision of ± 2 °C on each PZT was obtained, but the measurements used for the test were taken on one cycle (rising and dropping temperature) just after the database had been created, so the hysteretic effect had not a lot of influence on the results.

For the measurements on the fan cowl, a good precision is obtained for low temperatures (± 2 °C), but less precision is obtained for higher temperatures (see PZT 2 in Table 4 and PZT 1 in Table 5). Considering the results displayed in Table 3 and Fig. 4, it can be noticed that the higher the coefficient of variation α_C is, the more precision we get. Measurements on a too small range (7 °C) is not enough to get a robust evaluation of the linear regression coefficients. Further studies using a large heating zone will allow us to generate a larger and better controlled temperature variation for the database creation.

PZT transducers cannot be used as reliable temperature sensors since the temperature field can be estimated with a precision of ± 5 °C (Table 4 and Table 5), but this is enough for the targeted application that is robustifying SHM systems based on PZT and Lamb waves without adding supplementary temperature sensors.

Other features obtained from lamb wave measurements - such as time-of-arrival of the waves or the frequency shift of the transfer function - could also be used to have an estimation of the temperature field between two PZTs and increase the robustness of the temperature estimation and the number of sensing points on the structure.

Here, the static capacity is computed with impedance measurements on a large range of frequencies (from 20 to 60 kHz) whereas (Ilg et al., 2013) only considered a single measurement at 1 kHz . We could have used only one frequency for impedance measurements but using the mean on a range makes the static capacity measurement less prone to other temperature effect or presence of damage (Koo et al., 2008).

As pointed out by (Overly et al., 2009), it is important that the PZT are healthy to use this method because a damage or change in bonding conditions of the PZT will have an influence on the static capacity: C^0 for each PZT increases as the bonding is deteriorated and decreases when the PZT breaks, but the coefficient of temperature variation α_C is not really affected. The coefficients obtained for the PZT on the composite plate (Table 1) are quite similar compared to those of the test zone (Table 3). A small difference is accountable for the PZT dimensions considering (4). Differences between coefficients of identical PZTs is due to different boundary and ageing conditions and material anisotropy. For both structures, the coefficients of determination r^2 are high for every PZT, meaning that the linear regression is a good model (see Table 1 and Table 3). The experiments presented on the fan cowl deal with

temperatures between 15 and 50 °C which is less than the extreme temperatures reachable during operation. Tests on the small plate in an environmental chamber showed that the linear regression was accurate between -10 and $+100$ °C but the authors cannot guarantee that the linear regression is still a good model for temperatures exceeding this range.

6. CONCLUSION

Using measurements from the PZT for temperature estimation enables to get rid of supplementary temperature sensors and allows for a weight gain by using devices that are already mounted on the structure. The sensor network gives the opportunity to have a lot of sensing spots, leading to the imaging of the temperature field of the structure being monitored. Those temperature estimations can directly be used in the temperature compensation process of SHM measurements.

REFERENCES

Balmes, E., Guskov, M., Rebillat, M., Mechbal, N., 2014. Effects of temperature on the impedance of piezoelectric actuators used for SHM.

Fendzi, C., 2015. Contrôle Santé des Structures Composites: application à la Surveillance des Nacelles Aéronautiques. Paris, ENSAM.

Grisso, B.L., Inman, D.J., 2010. Temperature corrected sensor diagnostics for impedance-based SHM. *Journal of Sound and Vibration* 329, 2323–2336.

Ilg, J., Rupitsch, S.J., Lerch, R., 2013. Impedance-Based Temperature Sensing With Piezoceramic Devices. *IEEE Sensors Journal* 13, 2442–2449.

Konstantinidis, G., Drinkwater, B. and Wilcox, P., 2006. The temperature stability of guided wave structural health monitoring systems. *Smart Materials and Structures* 15(4), 967.Koo, K.-Y., Park, S., Lee, J.-J.,

Yun, C.-B., 2008. Automated Impedance-based Structural Health Monitoring Incorporating Effective Frequency Shift for Compensating Temperature Effects. *Journal of Intelligent Material Systems and Structures* 20, 367–377.

Lin, B., Giurgiutiu, V., Pollock, P., Xu, B., Doane, J., 2010. Durability and Survivability of Piezoelectric Wafer Active Sensors on Metallic Structure. *AIAA Journal* 48, 635–643.

Lize, E., Hudin, C., Guenard, N., Rebillat, M., Mechbal, N., Bolzmacher, C., 2016. Combination Of Frequency Shift And Impedance-Based Method For Robust Temperature Sensing Using Piezoceramic Devices For Shm.

Lu, Y. and Michaels, J. E., 2005. A methodology for structural health monitoring with diffuse ultrasonic waves in the presence of temperature variations. *Ultrasonics* 43(9), 717-731.

Marzani, A., Salamone, S., 2012. Numerical prediction and experimental verification of temperature effect on plate waves generated and received by piezoceramic sensors. *Mechanical Systems and Signal Processing* 30, 204–217.

Overly, T.G., Park, G., Farinholt, K.M., Farrar, C.R., 2009. Piezoelectric Active-Sensor Diagnostics and Validation Using Instantaneous Baseline Data. *IEEE Sensors Journal* 9, 1414–1421.

Park, G., Farrar, C.R., Rutherford, A.C., Robertson, A.N., 2006. Piezoelectric Active Sensor Self-Diagnostics Using Electrical Admittance Measurements. *Journal of Vibration and Acoustics* 128, 469.

Park, G., Sohn, H., Farrar, C.R., Inman, D.J., 2003. Overview of piezoelectric impedance-based health monitoring and path forward. *The Shock and Vibration Digest* 35 (6): 451–63.

Putkis, O., Dalton, R.P., Croxford, A.J., 2015. The influence of temperature variations on ultrasonic guided waves in anisotropic CFRP plates. *Ultrasonics* 60, 109–116.

Qing, X.P., Beard, S.J., Kumar, A., Sullivan, K., Aguilar, R., Merchant, M., Taniguchi, M., 2008. The performance of a piezoelectric-sensor-based SHM system under a combined cryogenic temperature and vibration environment. *Smart Materials and Structures* 17, 055010.

Sepehry, N., Shamshirsaz, M., Bastani, A., 2011. Experimental and theoretical analysis in impedance-based structural health monitoring with varying temperature. *Structural Health Monitoring* 10, 573–585.

Venu Gopal Madhav Annamdas, Chee Kiong Soh, 2010. Application of Electromechanical Impedance Technique for Engineering Structures: Review and Future Issues. *Journal of Intelligent Material Systems and Structures* 21, 41–59.

Wang, Y., Gao, L., Yuan, S., Qiu, L. and Qing, X., 2014. An adaptive filter-based temperature compensation technique for structural health monitoring. *Journal of Intelligent Material Systems and Structures* p. 1045389X13519001.

Yang, Y., Lim, Y.Y., Soh, C.K., 2008. Practical issues related to the application of the electromechanical impedance technique in the structural health monitoring of civil structures: I. Experiment. *Smart Materials and Structures* 17, 035008.

Yang, Y., Miao, A., 2008. Effect of External Vibration on PZT Impedance Signature. Sensors 8, 6846–6859.

Zhou, D., Kim, J.K., Ha, D.S., Quesenberry, J.D., Inman, D.J., 2009. A system approach for temperature dependency of impedance-based structural health monitoring. *Proc. SPIE*, 7293, 72930U-72930U-10